Materials Chemistry and Physics 334 (2025) 130511

Contents lists available at ScienceDirect

Materials Chemistry and Physics

journal homepage: www.elsevier.com/locate/matchemphys

Two novel Ti–Mo–Ta–Zr alloys for medical devices: Their microstructure, corrosion resistance and microhardness characteristics

Cristina Jiménez-Marcos [a], Julia Claudia Mirza-Rosca [a,b,*], Madalina Simona Baltatu [c], Petrica Vizureanu [c]

[a] Mechanical Engineering Department, Las Palmas de Gran Canaria University, Las Palmas de Gran Canaria, 35014, Spain
[b] Transilvania University of Brasov, Materials Engineering and Welding Department, Brasov, 500036, Romania
[c] Department of Technologies and Equipments for Materials Processing, Faculty of Materials Science and Engineering, Gheorghe Asachi Technical University of Iasi, Iasi, 700050, Romania

HIGHLIGHTS

- Two new titanium alloys with non-toxic elements and near β structure were analyzed.
- The passive film formed on the surface of both alloys is compact and protective.
- The increasing of Mo content significantly enhanced the corrosion resistance.

GRAPHICAL ABSTRACT

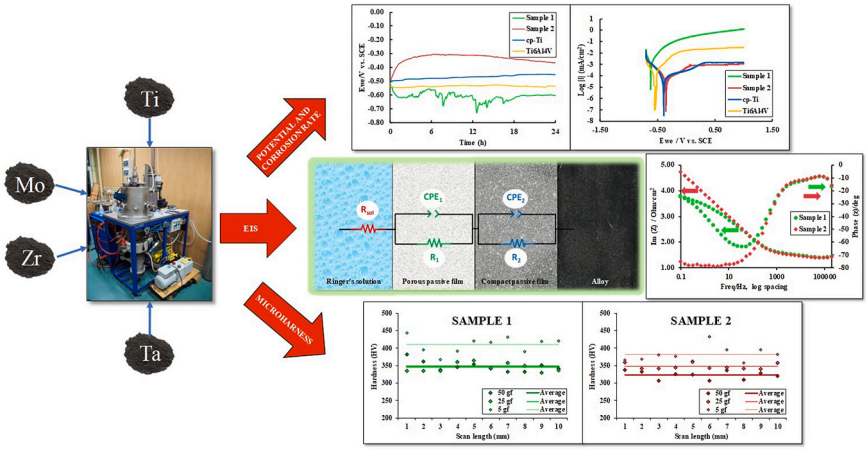

ARTICLE INFO

Keywords:
Titanium alloys
Microhardness testing
Corrosion resistance
Microstructural analysis

ABSTRACT

Titanium alloys have gained a solid reputation in the field of biomedicine due to their exceptional biocompatibility. However, it is important to note that some of these alloys do release toxic ions, which could potentially limit their application in sensitive scenarios. This study examines two new titanium alloys, TixMo15Ta7Zr (x = 15, 20 wt%) and it designed these alloys to overcome certain challenges by including helpful elements like molybdenum (Mo), tantalum (Ta) and zirconium (Zr). Advanced metallography, scanning electron microscopy, X-ray diffraction, microhardness measurements and electrochemical testing conclusively showed that the importantly elevated Mo content substantially improves corrosion resistance (with a corrosion rate value of 0.64 μm year^{-1}) by promoting the formation of an importantly more flexible passive layer, while simultaneously maintaining mechanical properties closely comparable to those of conventional titanium biomaterials possessing

* Corresponding author. Mechanical Engineering Department, Las Palmas de Gran Canaria University, Las Palmas de Gran Canaria, 35014, Spain.
E-mail addresses: julia.mirza@ulpgc.es, juliaclaudia.mirza@ulpgc.es (J.C. Mirza-Rosca).

https://doi.org/10.1016/j.matchemphys.2025.130511
Received 12 December 2024; Received in revised form 20 January 2025; Accepted 5 February 2025
Available online 6 February 2025

Vickers hardness values around 350 HV. These findings show that an important number of these alloys represent a revolutionary, promising solution for biomedical implants that are safer as well as more durable.

1. Introduction

Since its discovery by William Gregor in 1791, titanium has been recognized for its distinctive combination of strength, durability, and biocompatibility, which has made it a pivotal component in a diverse range of applications, including aerospace and modern medicine [1,2]. This metal is of particular value in the medical field, where it is utilized in orthopedic and dental implants, as well as an array of medical devices, due to its capacity to integrate with the human body without eliciting adverse reactions and it has the capacity to generate a passive film that serves as a protective barrier against external stimuli (TiO_2) [3].

However, the utilisation of commercial titanium alloys in biomedical applications is not without certain problems. Cp-Ti is recognized for its high biocompatibility, however, its mechanical and corrosion resistance in physiological environments is inadequate for numerous critical applications [4]. Additionally, the Ti–6Al–4V alloy utilized in orthopedic and dental implants has been linked to the development of allergies and other illnesses, including Alzheimer's and Parkinson's disease, due to the incorporation of aluminum (Al) and vanadium (V) [5,6]. In contrast, the Ti–6Al–7Nb alloy was developed to enhance biocompatibility and is employed in prosthetics and medical devices. However, it necessitates the presence of a robust protective coating [7,8]. Nitinol (TiNi), which is optimal for use in vascular stents and guidewires in minimally invasive surgery due to its capacity to revert to its original configuration, has the potential to release nickel, which can elicit allergic reactions and induce a range of cardiovascular and renal disorders [9].

To address these limitations, new titanium alloys composed of non-toxic elements such as Si, Ga, Zr, Ta and Mo, are under investigation. These elements have unique qualities that set them apart from commercial alloys, in addition to avoiding the dangers that come with using materials like Al, V, or Ni. One of the most important components of human biology is silicon, which is essential for the biological processes that promote the formation of new bone and connective tissues [10]. Gallium also reduces the risk of infections by exhibiting antibacterial qualities and contributing to biocompatibility [11]. Molybdenum, a β-stabilizing element with a low toxicity, has been studied for its potential to create Ti–Mo alloys, producing a stable oxide coating (MoO_3), preventing titanium corrosion, especially when present in optimized concentrations between 15 % and 20 %, improving the mechanical properties, and being thermally stable [12,13]. Tantalum is also a β-stabilizer that, at concentrations above 15 %, enhances biocompatibility, facilitating the formation of bone tissue around implants [14]. Zirconium is becoming a desired substitute for most medical applications, which contributes a combination of low elasticity and high corrosion resistance, ideal characteristics for biomedical applications [15]. The choice of these specific compositions responds to both previous findings and the need to combine biocompatibility, durability and superior mechanical properties.

When compared to previous Ti–Mo–Zr and Ti–Ta–Mo–Zr alloy systems, the TixMo15Ta7Zr alloys (where x can be 15 or 20 wt%) offer significant improvements. Even though Ti–Mo–Zr alloys showed improved resistance to corrosion, the addition of Ta to the new compositions improves biocompatibility even more, encouraging ideal integration with bone tissue and lowering the possibility of biological rejection. Furthermore, the Mo content, ranging from 15 % to 20 %, has been meticulously adjusted to ensure the formation of a more stable passive film, thereby surpassing the protective capabilities of earlier systems in simulated body fluids [16,17]. Finally, these alloys achieve an advanced balance between mechanical strength and elasticity, making them more suitable for critical applications than Ti–Ta–Mo–Zr systems, where elasticity was still limited.

The present study focuses on evaluating the corrosion behavior and mechanical properties of TixMo15Ta7Zr alloys in simulated body fluids, comparing them with reference materials such as Cp-Ti and Ti–6Al–4V, thereby completing our previous research [18]. A comparison of the new alloys with these reference materials reveals their superior corrosion resistance, enhanced biocompatibility, and their capacity to circumvent adverse reactions, such as those associated with the use of aluminum (Al) or vanadium (V). These compositions not only enhance the known properties of titanium, but also expand the possibilities for the design of more durable, safer, and more functional biomedical implants.

2. Experiment and methods

The following titanium alloys were subjected to investigation: Samples 1 and 2 were fabricated from pure elemental powders in a vacuum arc remelting (VAR) furnace. Sample 1 was composed of 63 % Ti, 15 % Mo, 7 % Zr, and 15 % Ta, while Sample 2 was composed of 58 Ti, 20 % Mo, 7 % Zr, and 15 % Ta. The purity of the elemental powders was greater than 99.90 %. A series of preliminary operations were conducted on the obtained ingots, including cutting and embedding them in epoxy resin. Then, the specimens were subjected to the polishing process at 150 rpm and 15 N of force utilizing the Struers TegraPol-11 polishing equipment (Copenhagen, Denmark). The progressive carbide abrasive papers with progressively higher grit were employed, ranging from P400 to P2500. Lastly, a 0.2 μm alumina suspension was employed on mirror-polishing cloths.

The samples were prepared for metallographic analysis in accordance with the standards set forth in ASTM E3-11(2017). The optical microscope Axio Vert.A1 MAT ZEISS (Jena, Germany) was utilized for the examination. Each sample was subjected to immersion in a solution of Kroll's reagent, which consists of 20 mL $C_2H_2O_2$, 30 mL HCl, and 10 mL HNO_3, for approximately 40 s. For elemental analysis, a Zeiss Sigma 300 VP scanning electron microscope (Carl Zeiss, Jena, Germany) was utilized in conjunction with an energy-dispersive X-ray spectrometer (EDX). For phase analysis of the materials, a Bruker D8 Advance X-ray diffraction (XRD) instrument was utilized. The research employed CuK radiation (1.5406 Å) with a step size of 0.02°, a current of 40 mA, and a power of 45 kV in the range of $2\theta = 10–80$.

Ten measurements, each lasting 15 s, were taken with the Future Tech FM-810 microhardness tester in compliance with ISO 14577–1:2015 for each load with the loads being 5, 25, and 50 gf, respectively. The observed diagonal lengths were then used by the iVicky application to automatically calculate the Vickers microhardness values.

In accordance with ISO 10271:2020, three electrodes were utilized for the electrochemical assessments: a working electrode (the specimen under examination), a counter electrode (a platinum electrode), and a reference electrode (a saturated calomel electrode). The area of each sample was determined using ImageJ software in order to conduct the experiments. The following components were quantified in mmol/L in the Ringer Grifols solution (Grifols Laboratories, Barcelona, Spain): The concentrations of the ions present in the solution were as follows: sodium (Na^+) 129.90 mmol/L; potassium (K^+) 5.40 mmol/L; chloride (Cl^-) 111.70 mmol/L; lactic acid ($C_3H_6O_3$) 27.20 mmol/L; and calcium (Ca^{2+}) 1.80 mmol/L. The corrosion behavior of the alloys was investigated employing a potentiostat-galvanostat BioLogic Essential SP-150 (Seyssinet-Pariset, France) in accordance with the following order: open circuit potential, linear polarization, and electrochemical impedance spectroscopy.

The 24-h open circuit potential of the study samples was determined

using the "E_{corr} vs. Time" method, as implemented in the EC-Lab program. In order to obtain the linear polarization curve, the surface area value and density of each sample were calculated. The potential scanning rate was 10.00 mV/min in the range from −0.70 V to 1.00 V vs. SCE. Impedance measurements were conducted using potentio electrochemical impedance spectroscopy, in accordance with ISO 16773–1:2016. The frequency range was set between 200 kHz and 100 mHz, and the data was displayed using Nyquist and Bode diagrams. Additionally, an electrochemical circuit was employed.

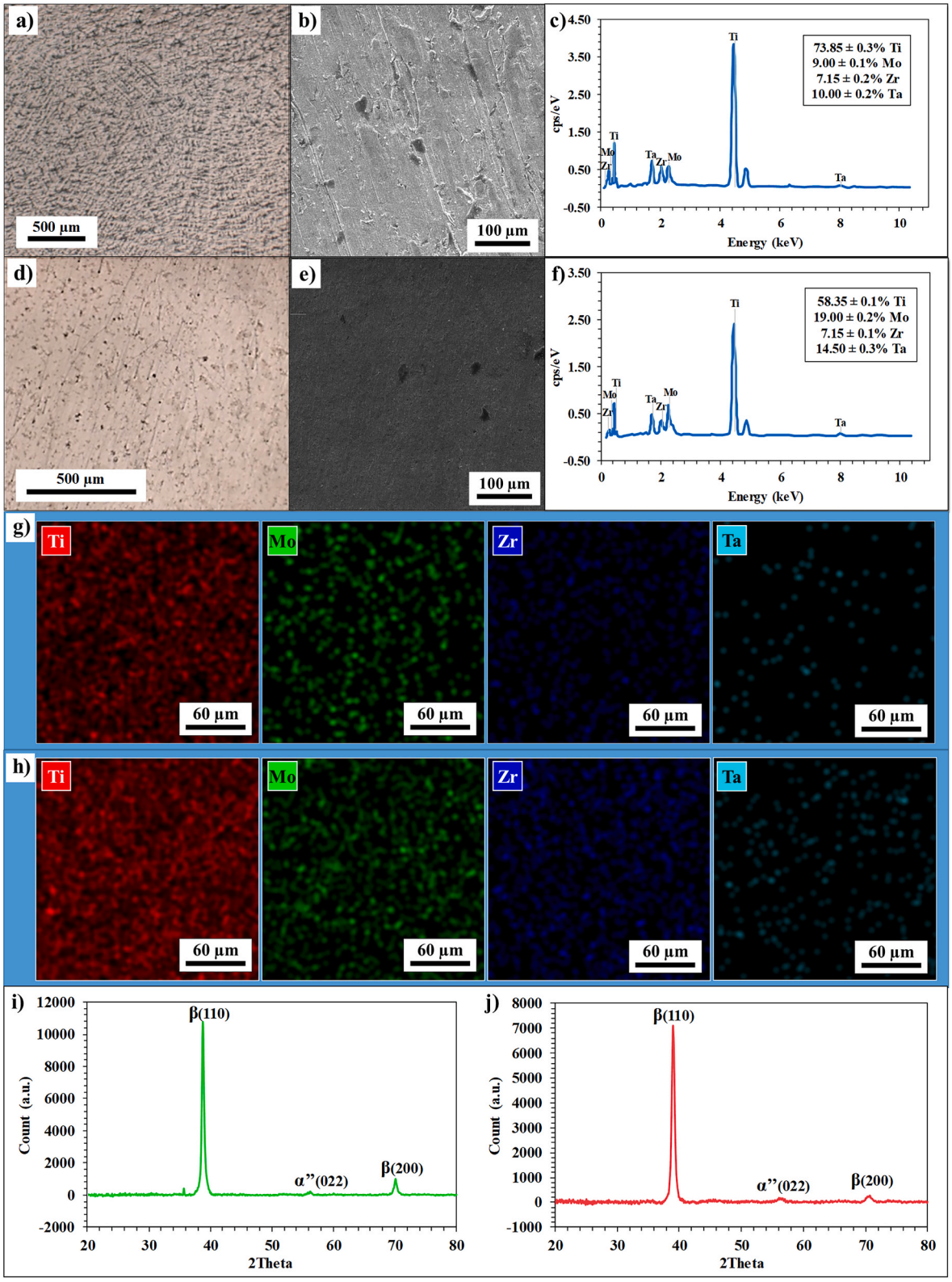

Fig. 1. Metallography (a, d), SEM image (b, e), EDX spectra and quantification (c, f), EDX elemental maps (g, h) and XRD spectra (i, j) for Sample 1 and Sample 2, respectively.

3. Results and discussion

The metallographic images of the two samples depicted in Fig. 1 illustrate a β lamellar microstructure with the presence of minor quantities of α phase, which can be attributed to the stabilizing influence of β-stabilizing elements, namely Zr and Ta. The point-specific EDX spectra and maps reveal the segregation of elements within the phases. This observation suggests that Mo also functions as an extremely effective stabilizer for the β solid solution. The stability of these features can be evaluated through the use of an Mo_{eq} equivalence assay. In accordance with the Mo equivalency formula (Mo_{eq} = Mo (wt.%) + Ta (wt.%)/4) [19], the Mo_{eq} values of the recently developed alloys demonstrate an increase as the Mo concentration rises. In particular, the Mo_{eq} values span a range of 18.75 %–23.75 %, which is considerably above the critical threshold of approximately 10 % for a stable β solid solution [20].

Fig. 2 displays the microhardness values HV0.005, HV0.025, and HV0.05 together with the mean, obtained from the 10 indentations made on each specimen. The application of 5 gf to each sample resulted in a considerable range of microhardness values, indicative of element segregation, reaching values between 380 and 410 HV (with standard deviation (SD) values of about ±22). However, at 25 or 50 gf, the indentations display greater uniformity for both samples and the values varies from 350 to 320 HV (with SD lower than ±15). These values were higher than those for Cp-Ti hardness and similar to those for Ti–6Al–4V (160–360 HV and 350–430, respectively) [21]. With increasing loading, the average depth of the footprint increased from approximately 0.9 nm–3.4 nm for both samples.

The open circuit potential curves of the studied samples, in addition to those of cp-Ti and Ti–6Al–4V, were analyzed over a 24-h testing period while the samples were submegerd in Ringer's solution (see Fig. 3a). The initial potential value of Sample 2 is −0.49 V, which is higher than that of Sample 1 due to the higher concentration of Mo (with a more anodic potential than Ti). The potential of Sample 1 exhibits oscillatory behavior during the test period, which can be attributed to the onset of localized corrosion. This process gives rise to alterations in the local environment, including changes in pH, chloride ion concentration, and oxygen availability. These fluctuations in the surrounding conditions, in turn, contribute to the observed fluctuations in the potential. It is possible that degradation and repassivation of the passive film on the alloy surface may occur in a repetitive cycle. This phenomenon could potentially lead to fluctuations in the open circuit potential, or OCP. Furthermore, the occurrence of anodic dissolution and cathodic reduction simultaneously can result in oscillatory behavior in the open circuit potential (OCP) if the system is not in a steady state. It can be observed that Sample 2 rapidly attained a stable potential of −0.27 V vs. SCE. The concentration of Mo has been demonstrated to influence the thickness, composition, and stability of the protective passive oxide film that forms on the surface of the alloy [22]. In the case of cp-Ti and Ti6Al4V, it is evident that they exhibit a tendency to stabilise their potential over the 24-h testing period.

Fig. 3b illustrates the outcomes of the linear polarization technique employed to ascertain the corrosion rate of the alloys, cp-Ti and Ti6Al4V, plotted on a semi-logarithmic scale. It can be observed that the passive range is considerable for Sample 2, indicating that the passive layer is stable and effective. The corrosion rate, V_{corr}) was found to be lower for Sample 2 (0.64 μm $year^{-1}$) in comparison to that of Sample 1 (9.95 μm $year^{-1}$) and the V_{corr} of Ti6Al4V (0.73 μm $year^{-1}$). Furthermore, the polarization resistance (R_p) of 10^6 Ohm·cm^2 was notably high for new titanium alloys, indicating that they possess considerable corrosion resistance.

The bigger capacitive arc for Sample 2 is indicative of a greater charge transfer resistance (R_{ct}), as shown in Fig. 4a. This result suggests a more effective passive film, which may be attributed to the alloy's optimal composition. Mo and Ta promote the formation of a compact inner layer, whereas Zr improves overall corrosion resistance. It has been shown that by blocking the flow of ions and electrons across the contact, this passive layer slows down the dissolution processes of the underlying metal. In biomedical applications, this enhanced durability and reduced release of hazardous metal ions are crucial characteristics that promote implant safety and reliability.

With a higher Mo concentration than Sample 1, Sample 2 demonstrated better corrosion resistance, suggesting a more effective and durable protective layer. Fig. 4b illustrates the impedance and Bode phase diagrams, which represent the logarithm of the impedance values (primary axis) and phase angles (secondary axis) as a function of frequency. The Bode impedance plot showed a higher impedance modulus value in Sample 2, reaching 56 kΩ cm^2 in the low-frequency region, indicating higher resistance to charge transfer or lower ionic conductivity through the passive film. Sample 2 also showed a higher maximum phase angle of 78.7° over a wider frequency range, indicating a more capacitive response, characteristic of a compact and stable passive layer. This higher capacitance reflects the system's ability to store electrical charge, which is related to the quality and homogeneity of the passive film formed. The presence of Mo, which promotes the creation of a thick and stable oxide film (MoO_3), and the combined effects of Ta and Zr, which increase mechanical strength and corrosion resistance, are responsible for Sample 2's passive layer's robustness. This capacitive characteristic strengthens corrosion resistance and durability, which is especially important for biological applications that need long-term stability. In order to gain a more nuanced understanding of the corrosion layer structure and characteristics, a computational model based on the equivalent electrical circuit (EEC) was employed to simulate the impedance spectra, as illustrated in Fig. 4c. The main parameters derived from the fitting using ZSimpWin software are as follows: R_{sol} represents the solution resistance, and two parallel pairs, R_1/CPE_1 and R_2/CPE_2, correspond to the porous and compact passive layer (see Fig. 4c). It was states that the inner barrier layer is created by the inward

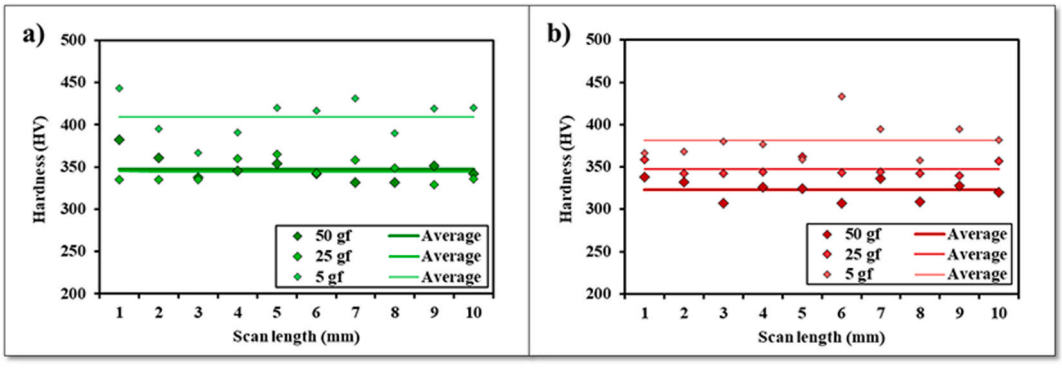

Fig. 2. Microhardness results of a) Sample 1 and Sample b).

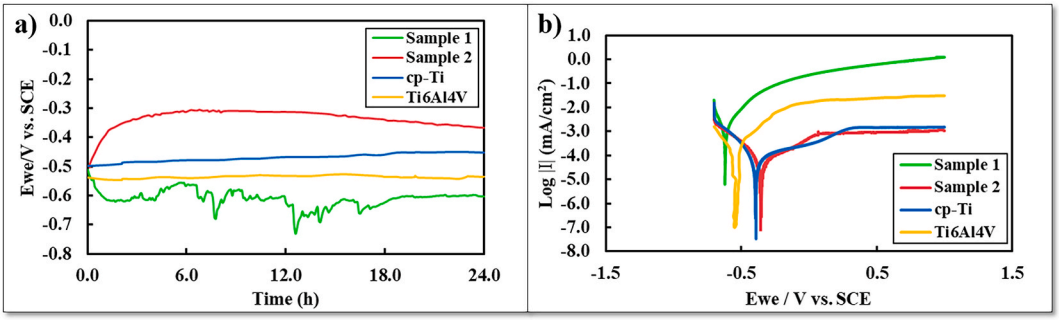

Fig. 3. a) Open circuit potential after 24 h' immersion time; b) linear polarization curves.

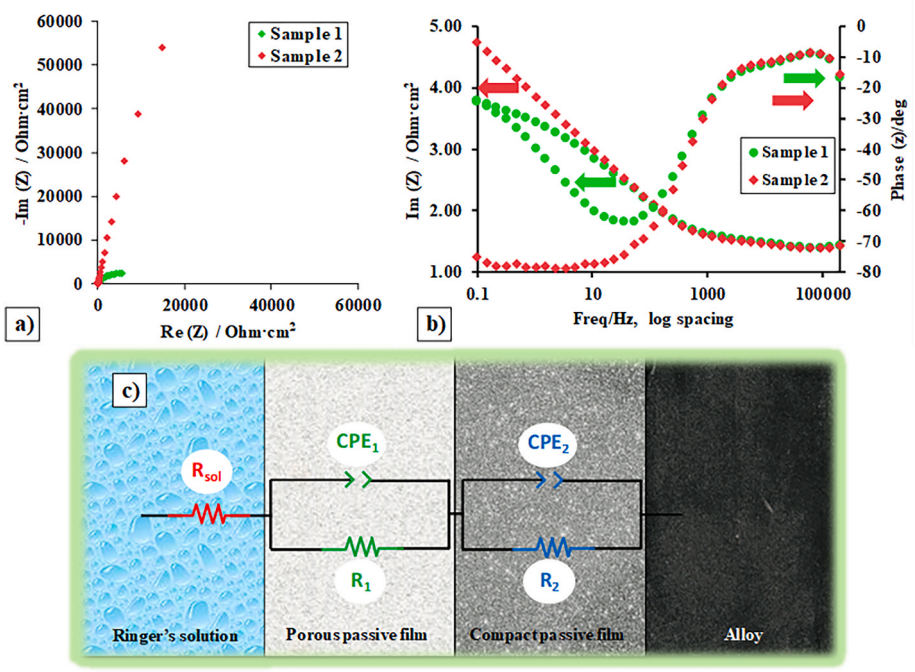

Fig. 4. a) Nyquist, b) Bode-IZI and Bode-phase diagrams at E_{corr}, c) equivalent circuit.

transition of oxygen ions and the outer porous layer is formed by the hydrolysis of cations flowing from the inner barrier layer [23,24]. The use of a constant phase element (CPE) in place of pure capacitance serves to highlight the non-ideal capacitive response, which is a consequence of the heterogeneous nature of the passive film in alloys. The electrical impedance of the CPE can be determined using the following equation [25]:

$$Z_{CPE} = Y^{-1}(jw)^{-n} \quad (1)$$

In this context, Y represents a constant with dimensions of $\Omega^{-1}\cdot s^n$, which is also known as the CPE coefficient or pseudo-capacitance. The imaginary unit, j, is defined as $j^2 = -1$, while ω denotes the angular frequency. Finally, n is the CPE exponent, with $0 \leq n \leq 1$. When $n = 1$, the CPE behaves like an ideal capacitor. Conversely, when $n = 0$, it behaves like a pure resistor.

The parameters extracted from the fitting of the experimental data are presented in Table 1. It has been demonstrated that the enhanced resistance of the inner compact passive layer (R_2 or R_{ct}) in Sample 2, which is approximately 8 times higher than in Sample 1, underscores the capacity of this alloy to establish an effective barrier against corrosion. In general, the corrosion resistance ($R_p = R_1 + R_2$) is higher for Sample 2, reaching values up to 10^5 Ohm·cm^2. This finding is particularly significant in physiological environments, where the stability of the inner passive layer is imperative to avert the release of metal ions. The higher compactness of this layer (n_2 close to 1) in Sample 2 suggests that the film is less susceptible to diffusion processes, resulting in prolonged protection. In comparison, the diffusive behavior observed in Sample 1 (n_1 close to 0.5) and its thicker outer layer (smaller Y_1) could indicate a lower overall protection efficiency. These observations, attributable to the Mo content, underscore the necessity of optimizing the chemical composition to ensure the optimal performance of these alloys in critical applications, such as biomedical implants, where corrosion resistance and structural integrity are essential. During exposure to simulated body fluid, Mo is oxidized to Mo^{+4} (MoO_2) and Mo^{+6} (MoO_3 and MoO_4^{2-}), following the reactions:

Table 1
Equivalent electric circuit parameters for fitting the experimental EIS data.

Parameters	Sample 1	Sample 2
Y_1 (Ohm·cm^2)	$3.93\cdot10^{-5}$	$1.20\cdot10^{-4}$
n_1	0.97	0.48
R_1 (Ohm·cm^2)	$1.41\cdot10^{3}$	19.48
Y_2 (S·sec^n/cm^2)	$1.03\cdot10^{-4}$	$2.28\cdot10^{-5}$
n_2	0.68	0.88
R_2 (Ohm·cm^2)	$1.03\cdot10^{4}$	$8.60\cdot10^{5}$
χ^2	$7.14\cdot10^{-3}$	$8.56\cdot10^{-4}$

$$Mo + 2H_2O \rightarrow MoO_2 + 4H^+ + 4e^- \quad (2)$$

The compound of hexavalent molybdenum is very important; is illustrated by molybdenum trioxide and by its ionic form:

$$MoO_2 + H_2O \rightarrow MoO_3 + 2H^+ + 2e^- \quad (3)$$

$$MoO_2 + 2H_2O \rightarrow MoO_4^{2-} + 4H^+ + 2e^- \quad (4)$$

The same phenomenom occurs with Ta:

$$2Ta + 5H_2O \rightarrow Ta_2O_5 + 10H^+ + 10e^- \quad (5)$$

4. Conclusions

This study examined the corrosion behavior and microstructural characteristics of two recently developed titanium alloys containing biocompatible elements (Mo, Zr, and Ta). The alloy with a higher Mo content displays enhanced corrosion resistance due to a more robust passive layer. The microhardness values of both alloys are consistent with those of commonly used Ti biomaterials, indicating uniformity and good mechanical performance. These findings substantiate the potential of these novel, presumably non-toxic titanium alloys as promising candidates for biomedical applications.

Future research should concentrate on an extensive investigation of higher Mo content, integrating alloy manufacturing, improved characterization, mechanical and electrochemical evaluations, and biocompatibility analyses. By progressively increasing Mo content and refining the alloy composition, one may methodically assess the tradeoffs and advantages, hence facilitating the advancement of superior titanium alloys for clinical applications.

CRediT authorship contribution statement

Cristina Jiménez-Marcos: Writing – original draft, Investigation, Formal analysis. **Julia Claudia Mirza-Rosca:** Writing – review & editing, Validation, Supervision. **Madalina Simona Baltatu:** Resources, Methodology, Conceptualization. **Petrica Vizureanu:** Writing – review & editing, Supervision, Resources.

Declaration of competing interest

The authors declare that they have no known competing financial interests or personal relationships that could have appeared to influence the work reported in this paper.

Acknowledgements

We hereby acknowledge the European project 2023-1-RO01-KA220-HED-000159985: Smart Healthcare Engineering and the project Cabildo22-01.

Data availability

Data will be made available on request.

References

[1] Y. Zhang, K. Chu, S. He, B. Wang, W. Zhu, F. Ren, Fabrication of high strength, antibacterial and biocompatible Ti-5Mo-5Ag alloy for medical and surgical implant applications, Mater. Sci. Eng. C. 106 (2020) 110165, https://doi.org/10.1016/J.MSEC.2019.110165.

[2] W. Abd-Elaziem, M.A. Darwish, A. Hamada, W.M. Daoush, Titanium-Based alloys and composites for orthopedic implants Applications: a comprehensive review, Mater. Des. 241 (2024) 112850, https://doi.org/10.1016/j.matdes.2024.112850.

[3] B. Wu, Y. Tang, K. Wang, X. Zhou, L. Xiang, Nanostructured titanium implant surface facilitating osseointegration from protein adsorption to osteogenesis: the example of TiO2 NTAs, Int. J. Nanomed. 17 (2022) 1865–1879, https://doi.org/10.2147/IJN.S362720.

[4] M. Najafizadeh, S. Yazdi, M. Bozorg, M. Ghasempour-Mouziraji, M. Hosseinzadeh, M. Zarrabian, P. Cavaliere, Classification and applications of titanium and its alloys: a review, J. Alloy. Compd. Commun. 3 (2024) 100019, https://doi.org/10.1016/j.jacomc.2024.100019.

[5] G. Senopati, R.A. Rahman Rashid, I. Kartika, S. Palanisamy, Recent development of low-cost β-Ti alloys for biomedical applications: a review, Metals 13 (2023), https://doi.org/10.3390/met13020194.

[6] J. Dias Corpa Tardelli, C. Bolfarini, A. Cândido dos Reis, Comparative analysis of corrosion resistance between beta titanium and Ti-6Al-4V alloys: a systematic review, J. Trace Elem. Med. Biol. 62 (2020) 126618, https://doi.org/10.1016/j.jtemb.2020.126618.

[7] M.V. Popa, D. Raducanu, E. Vasilescu, P. Drob, D. Cojocaru, C. Vasilescu, S. Ivanescu, J.C.M. Rosca, Mechanical and corrosion behaviour of a Ti-Al-Nb alloy after deformation at elevated temperatures, Mater. Corros. 59 (2008) 919–928, https://doi.org/10.1002/maco.200805003.

[8] Ş. Culfa, S.M. Toker, Interaction of Ti-6Al-7Nb alloy with simulated body fluid; a preliminary biocompatibility investigation, Front. Life Sci. Relat. Technol. 4 (2023) 111–117, https://doi.org/10.51753/flsrt.1294479.

[9] G. Genchi, A. Carocci, G. Lauria, M.S. Sinicropi, A. Catalano, Nickel: human health and environmental toxicology, Int. J. Environ. Res. Publ. Health 17 (2020) 679, https://doi.org/10.3390/ijerph17030679.

[10] A. Bordbar-Khiabani, M. Gasik, Electrochemical and biological characterization of Ti–Nb–Zr–Si alloy for orthopedic applications, Sci. Rep. 13 (2023) 2312, https://doi.org/10.1038/s41598-023-29553-5.

[11] R. McHendrie, N.H. Nguyen, M.T. Nguyen, K. Fallahnezhad, K. Vasilev, V. K. Truong, R. Hashemi, Development of novel antibacterial Ti-Nb-Ga alloys with low stiffness for medical implant applications, J. Funct. Biomater. 15 (2024) 167, https://doi.org/10.3390/jfb15060167.

[12] Q. Chen, G.A. Thouas, Metallic implant biomaterials, Mater. Sci. Eng. R Rep. 87 (2015) 1–57, https://doi.org/10.1016/j.mser.2014.10.001.

[13] A.H. Awad, M. Saood, H.A. Aly, A.W. Abdelghany, Role of Mo and Zr additions in enhancing the behavior of new Ti–Mo alloys for implant materials, Met. Mater. Int. (2024), https://doi.org/10.1007/s12540-024-01813-7.

[14] S. Bălțatu, P. Vizureanu, D. Mareci, L.C. Burtan, C. Chiruță, L.C. Trincă, Effect of Ta on the electrochemical behavior of new TiMoZrTa alloys in artificial physiological solution simulating in vitro inflammatory conditions, Mater. Corros. 67 (2016) 1314–1320, https://doi.org/10.1002/maco.201609041.

[15] C. Jimenez-Marcos, J.C. Mirza-Rosca, M.S. Baltatu, P. Vizureanu, Experimental research on new developed titanium alloys for biomedical applications, Bioengineering 9 (2022) 686, https://doi.org/10.3390/bioengineering9110686.

[16] E.-B. Lee, M.-K. Han, B.-J. Kim, H.-J. Song, Y.-J. Park, Effect of molybdenum on the microstructure, mechanical properties and corrosion behavior of Ti alloys, Int. J. Mater. Res. 105 (2014) 847–853, https://doi.org/10.3139/146.111092.

[17] K. Glowka, M. Zubko, P. Świec, K. Prusik, M. Szklarska, D. Chrobak, J.L. Lábár, D. Stróż, Influence of molybdenum on the microstructure, mechanical properties and corrosion resistance of Ti20Ta20Nb20(ZrHf)20−xMox (where: x = 0, 5, 10, 15, 20) high entropy alloys, Materials 15 (2022) 393, https://doi.org/10.3390/ma15010393.

[18] M.S. Baltatu, M.C. Spataru, L. Verestiuc, V. Balan, C. Solcan, A.V. Sandu, V. Geanta, I. Voiculescu, P. Vizureanu, Design, synthesis, and preliminary evaluation for Ti-Mo-Zr-Ta-Si alloys for potential implant applications, Materials 14 (2021) 6806, https://doi.org/10.3390/MA14226806.

[19] W. Weng, A. Biesiekierski, J. Lin, Y. Li, C. Wen, Impact of rare earth elements on nanohardness and nanowear properties of beta-type Ti-24Nb-38Zr-2Mo alloy for medical applications, Materialia 12 (2020) 100772, https://doi.org/10.1016/j.mtla.2020.100772.

[20] W. Bai, G. Xu, M. Tan, Z. Yang, L. Zeng, D. Wu, L. Liu, L. Zhang, Diffusivities and atomic mobilities in bcc Ti-Mo-Zr alloys, Materials 11 (2018) 1909, https://doi.org/10.3390/ma11101909.

[21] P.A. Lopes, A.F.P. Carreiro, R.M. Nascimento, B.R. Vahey, B. Henriques, J.C. M. Souza, Physicochemical and Microscopic Characterization of Implant – Abutment Joints, 2019, pp. 100–104, https://doi.org/10.4103/ejd.ejd.

[22] J. Zhang, C. Wang, N. Shareef, Microstructure and properties of Ti-Zr-Mo alloys fabricated by laser directed energy deposition, Materials 16 (2023) 1054, https://doi.org/10.3390/ma16031054.

[23] Y.-W. Cui, L.-Y. Chen, P. Qin, R. Li, Q. Zang, J. Peng, L. Zhang, S. Lu, L. Wang, L.-C. Zhang, Metastable pitting corrosion behavior of laser powder bed fusion produced Ti-6Al-4V in Hank's solution, Corros. Sci. 203 (2022) 110333, https://doi.org/10.1016/j.corsci.2022.110333.

[24] H. Liu, Z.-X. Wang, J. Cheng, N. Li, S.-X. Liang, L. Zhang, F. Shang, D. Oleksandr, L.-Y. Chen, Nb-content-dependent passivation behavior of Ti–Nb alloys for biomedical applications, J. Mater. Res. Technol. 27 (2023) 7882–7894, https://doi.org/10.1016/j.jmrt.2023.11.203.

[25] B.A. Boukamp, A Nonlinear Least Squares Fit procedure for analysis of immittance data of electrochemical systems, Solid State Ionics 20 (1986) 31–44, https://doi.org/10.1016/0167-2738(86)90031-7.